



OPEN ACCESS

EDITED BY
Roberto Cerbino,
University of Vienna, Austria

REVIEWED BY
Marco Laurati,
University of Florence, Italy
Silvia Corezzi,
University of Perugia, Italy

*CORRESPONDENCE
C. Haro-Pérez,
cehp@azc.uam.mx
L. F. Rojas-Ochoa,
luisf.rojas@cinvestav.mx

SPECIALTY SECTION
This article was submitted to Soft Matter
Physics,
a section of the journal
Frontiers in Physics

RECEIVED 07 July 2022
ACCEPTED 10 August 2022
PUBLISHED 08 September 2022

CITATION
Bocanegra-Flores J, Haro-Pérez C,
Reyes-Contreras D and Rojas-Ochoa LF
(2022), Crystallization kinetics of
charged PNIPAM microgels dispersions
at low volume fractions.
Front. Phys. 10:988903.
doi: 10.3389/fphy.2022.988903

COPYRIGHT
© 2022 Bocanegra-Flores, Haro-Pérez,
Reyes-Contreras and Rojas-Ochoa.
This is an open-access article
distributed under the terms of the
[Creative Commons Attribution License
\(CC BY\)](https://creativecommons.org/licenses/by/4.0/). The use, distribution or
reproduction in other forums is
permitted, provided the original
author(s) and the copyright owner(s) are
credited and that the original
publication in this journal is cited, in
accordance with accepted academic
practice. No use, distribution or
reproduction is permitted which does
not comply with these terms.

Crystallization kinetics of charged PNIPAM microgels dispersions at low volume fractions

J. Bocanegra-Flores¹, C. Haro-Pérez^{2*}, D. Reyes-Contreras³
and L. F. Rojas-Ochoa^{1*}

¹Departamento de Física, CINVESTAV-IPN, Av. Instituto Politécnico Nacional 2508, Mexico City, Mexico, ²Departamento de Ciencias Básicas, Universidad Autónoma Metropolitana-Azcapotzalco, Mexico City, Mexico, ³Facultad de Ciencias, Campus El Cerrillo, Universidad Autónoma del Estado de México, Toluca, Mexico

This work studies the kinetics of crystallization of charged microgels suspensions of Poly-N-Isopropylacrylamide (PNIPAM) at low ionic strength. The liquid-crystal transition is induced by suddenly decreasing the temperature of the microgel dispersion, and the crystallization process is monitored by measuring the temporal evolution of the static structure factor of the dispersion using light scattering. We find that the crystal growth rate, indicated by the temporal evolution of the crystallinity factor, strongly depends on the quenching temperature.

KEYWORDS

colloidal crystallization, microgels, PNIPAM, light scattering, charged colloids

Introduction

Microgels dispersions are unique since they respond to different stimuli, such as temperature, pH, ionic strength, and solvent [1–3]. The size of thermosensitive microgels, such as PNIPAM microgels, can be tuned by changing the temperature. At low temperatures, the microgels are swollen, and the effective particle density is very similar to that of the solvent. As the temperature increases, the microgel size decreases slowly until the Lower Critical Solution Temperature (LCST) is reached, provoking a sudden coil-to-globule transition of the constituent polymer chains that translates into a particle volume phase transition (VPT). For charged microgels, dispersions are colloidally stable even beyond the LCST due to electrostatic stabilization [4]. We can take advantage of this property to study various physical phenomena that occur as a function of temperature in microgel dispersions [2, 3, 5–7]. The temperature affects the particle size, softness, permeability and charge density, implying a temperature-dependent interaction potential [4, 8, 9]. Thanks to this, a microgel dispersion can undergo, for example, a phase transition from liquid to crystal by changing the temperature [4]. Temperature is maybe one of the parameters that experimentalists can better control. Phase transitions such as melting [10] and crystallization [5, 11, 12] are still open questions. For example, crystallization kinetics

in atomic systems is complicated to follow due to the requirement of high temporal and atomic spatial resolutions [13]. However, colloidal systems, composed of particles of larger sizes, such as microgel dispersions, provide the possibility to follow physical phenomena such as crystallization in time. Moreover, the possibility of controlling the particle pair-interaction in colloids makes them very attractive. In particular, the peculiarity of microgel systems allows for tuning the particle interaction potential by changing the temperature and, consequently, inducing crystallization in a controlled way [14, 15]. This characteristic may be of great interest in material science to design, for example, photonic materials made of thermosensitive microgels [5, 16–18]. In case of ionic microgels, the presence of charged groups can also induce interesting responsiveness to other parameters, such as pH and, by controlling its temporal profile, microgel dispersions can be programmed to melt or crystallize [19]. Charged groups are frequently present in PNIPAM microgels due to the use of an ionic initiator or an ionic comonomer [20]. Pure PNIPAM microgels are frequently considered neutral, but their residual charge may significantly affect their colloidal behavior, mainly at low salt concentrations and/or high-volume fractions [19, 21–23]. Here, thanks to the long-range interaction potential among charged PNIPAM microgels at deionized conditions, we study the crystallization of microgel systems at low particle number concentrations and the influence of temperature on the crystallization kinetics in contrast to previous studies, where very high-volume fractions were used [11]. The crystallization process is followed by measuring the sample structure time-evolution by light scattering.

Materials and methods

Microgel synthesis and sample preparation

The PNIPAM microgels under study are synthesized by polymerization precipitation as described in Ref. [24]. First, the monomer (NIPAM), the crosslinker (bisacrylamide, BIS), and the surfactant (sodium dodecyl sulfate, SDS) are dissolved in 450 ml of water in a three-mouth round bottom flask, purged with nitrogen during 30 min and heated to 70°C. Then, in another recipient, the initiator, (potassium persulfate, KPS), is dissolved in 50 ml of water and purged with nitrogen for 30 min. Then, the initiator solution is injected into the monomer solution, and the sample is kept under continuous stirring. After 5 h, the solution is left to cool down to room temperature. Finally, the microgel dispersion is filtered through glass wool, dialyzed for 2 weeks, and centrifuged ten times. In each centrifugation step, the supernatant is removed, and the microgels are redispersed in ultrapure water.

We perform the crystallization study with two types of microgels having different electrostatic charges, and this is achieved by using a different initiator concentration in the microgel synthesis. The quantities of reactants used in each synthesis are shown in Table 1. Once the microgel dispersion is purified, the weight fraction is obtained from weighing a specific volume of microgel dispersion before and after drying. The weight fraction was obtained for six samples, the average value is reported in Table 1, and the error is the sample standard deviation. The resulting weight fractions, shown in Table 1, are 3.17% [(128 ± 3) particles/μm³] and 1.1% [(19 ± 2) particles/μm³] for the KPS0.1 and KPS0.6 systems, respectively. The number particle concentration of each microgel stock is obtained by following the procedure described in [4]. First, several samples are prepared by dilution of the stock solution and deionized to maximize particle electrostatic repulsion. At ambient temperature, most of the samples crystallize and show Bragg peaks whose relative positions indicate the appearance of a BCC lattice. Then, from the main peak position, the particle concentration of each sample is obtained by using [25].

$$n = \left(\frac{2\sqrt{2}\mu}{\sqrt{2}\lambda} \right)^3 \sin^3 \left(\frac{\theta_{\max}}{2} \right) \quad (1)$$

μ is the refractive index of the solvent, λ is the wavelength of the laser used in the light scattering experiments, and θ_{\max} is the angular position of the main peak of the structure factor. Finally, the particle number density of the stock solution is obtained by multiplying the concentration of each sample by the dilution factor used to prepare it. In Table 1 we report the average values of the particle number concentration for each stock solution.

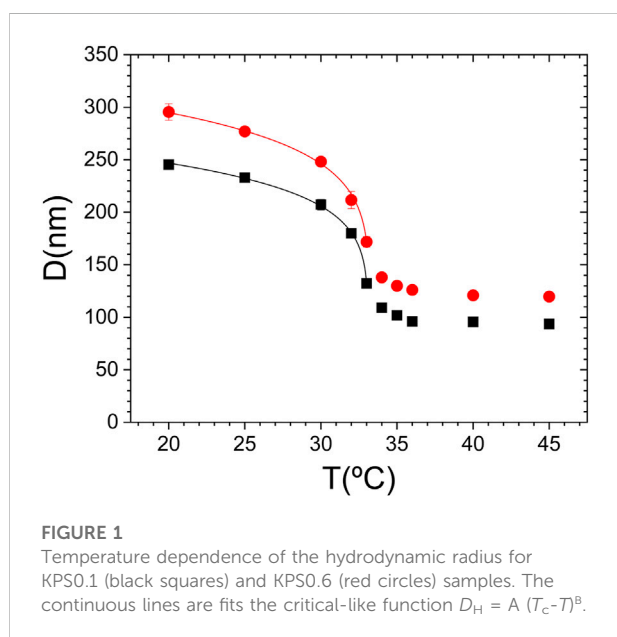
Once the stock solution concentration is known, the system was prepared by dilution with ultrapure water to the desired concentration and placed in cylindrical quartz cells with ionic exchanger resins (Amberlite IRN-150) to deionize the sample completely. After that, the cells were sealed to avoid contact with air.

Light scattering experiments

The system crystallization kinetics was followed by measuring the static structure factor of the microgel dispersions by static light scattering. The device used to perform the experiments is a 3D-DLS spectrometer [26–28] (LS Instruments, Switzerland) provided with a laser working at 632.8 nm and two avalanche photodiodes. In this device, it is possible to perform two light scattering experiments simultaneously with the same wavevector. Cross-correlating the scattered signals from both experiments makes possible the suppression of multiple scattering from the total intensity impinging on the detectors. The static structure factor is

TABLE 1 Reactants used in synthesizing 500 ml of PNIPAM microgel dispersion, the weight fraction, and the particle number density of the resulting stock microgel dispersions.

System	NIPAM (g)	BIS (g)	KPS (g)	SDS (g)	W/W (%)	n (pp/ μm^3)
KPS0.1	7.87	0.15	0.1	0.15	3.17 \pm 0.06	128 \pm 3
KPS0.6	7.87	0.15	0.6	0.15	1.10 \pm 0.02	19 \pm 2



obtained by dividing the intensity scattered by the correlated sample by that scattered by a very diluted sample where particle interactions are absent; see further details in Ref. [29].

Before light scattering experiments, the samples were heated up to 45°C. They were kept at this temperature for 10 min to ensure all the samples were in a fluid state. After that, the quenching was performed by introducing the samples into the decalin bath located in the light scattering device at a temperature lower than the microgel volume phase transition temperature (VPTT); a thermostat controls the bath temperature. We measure the sample structure's time evolution after 10 min to follow its crystallization. The sample was steadily rotated during the experiments to obtain the ensemble-averaged intensity since the crystalline samples are non-ergodic. The temperatures used to do the quenching are 20°C, 25°C, and 30°C. At all these temperatures, the microgel dispersions crystallize. The microgel size was obtained by dynamic light scattering using a diluted sample. Here, the sample prepared at a high dilution was equilibrated at the desired temperature, and the free diffusion coefficient, D_0 , was obtained from a second cumulant fit to the measured scattered field correlation function [30]. Finally, we calculate

the hydrodynamic radius, a , by applying the Stokes-Einstein relation, $D_0 = \kappa_B T / (6\pi\eta a)$, where κ_B is the Boltzmann constant, T the temperature, and η the solvent viscosity [31].

Results and discussion

Before the crystallization experiments, the temperature dependence of the microgel size was measured by dynamic (DLS) and static light scattering (SLS). From DLS measurements, we can see that both microgel systems, KPS0.1 and KPS0.6, show the typical thermosensitive behavior of PNIPAM, as shown in Figure 1, where the temperature dependence of the hydrodynamic diameter of both systems is shown. The microgels display a swollen conformation and a larger particle diameter at low temperatures. As the temperature increases, the microgel expels water from inside and thus monotonously decreases its size. PNIPAM is hydrophobic at high temperatures, so microgels size decreases suddenly at temperatures above but close to the LCST. The measured temperature dependent hydrodynamic size is fitted to the critical-like function $D_H = A * (LCST - T)^B$ to determine the LCST of each microgel, obtaining that the LCST is $(33.09 \pm 0.02)^\circ\text{C}$, and $(33.19 \pm 0.09)^\circ\text{C}$ for KPS0.1 and KPS0.6 system, respectively. The fits are shown in Figure 1 as continuous lines. Besides the similarity of the LCST values obtained for both microgels, they also display similar sizes at all temperatures. However, the most charged microgels display sizes slightly larger, probably due to the higher electrostatic repulsion between the ionized groups in the polymer chains that compose the particles. Note that the microgels are colloidally stable even beyond the LCST due to the electrostatic stabilization provided by the ionic initiator used in the synthesis. The presence of a small fraction of sulphate groups, originated by the KPS initiator, provides the microgel with a negative charge, whose presence has also been confirmed by electrophoretic mobility experiments [32, 33].

Once the thermosensitive behavior and particle dimensions are known, we characterize the microgel dispersion static structure at different particle concentrations at a temperature beyond the VPTT for both systems at deionized conditions. Figure 2A) shows the results for the KPS0.1 system, and Figure 2B) for the KPS0.6,

respectively. In both cases, the samples are in the fluid state for the concentrations shown in the figures.

Figure 2 shows the principal structural peak related to neighboring interparticle correlations and successive damped peaks. Moreover, as expected for charged colloids at low ionic strengths, the primary peak shifts to higher q -values as particle concentration increases following a one-third power law [34, 35], as seen in the insets. Here, the main peak position of the experimental $S(q)$ is plotted as a function of the dilution factor used to prepare the different systems from the stock solution on a log-log scale. We use the same color code in the inset as in the main figure, and blue symbols correspond to additional samples studied to span the concentration interval. The dashed lines are linear fits to the experiments, and their slopes are -0.34 and -0.33, agreeing with the expected $-1/3$ value. This means that particles arrange to maximize distances due to the electrostatic repulsion among them. Moreover, all structure factors display the typical short-range order present in liquids as confirmed by the agreement between experiments (symbols) and the theoretical $S(q)$'s (lines) obtained from liquid state theory by solving the Ornstein-Zernike equation using the hypernetted chain (HNC) closure relation, and assuming a Yukawa-like particle interaction potential [36],

$$U(r) = \frac{Z_{\text{eff}}^2 e^2}{4\pi\epsilon_0\epsilon_r} \left(\frac{\exp(\kappa a)}{1 + \kappa a} \right)^2 \frac{\exp(-\kappa r)}{r} \quad (2)$$

where, Z_{eff} is an effective charge, e the electron charge, κ the effective inverse Debye screening length, a the particle radius, ϵ_0 the vacuum dielectric constant, ϵ_r the relative solvent-vacuum dielectric constant, and r the particle-particle center distance. Since the systems are deionized, we calculate the theoretical $S(q)$'s by fixing the salt concentration to 10^{-7} M and assuming monodisperse systems. The only fitting parameters are the particle effective charge, and the number concentration, n . The n needed to perform all the fits only differs up to 5% from that corresponding to the stock solution divided by the dilution factor, which corroborates the initially estimated particle concentration. We find that the effective particle charge slightly varies with particle concentration in the investigated concentration interval, and its value is around 420 for KPS0.1 system, and 470 for KPS0.6 system. It is convenient to point out that, even though the influence of the electrostatic charge of PNIPAM microgels is often neglected in many studies, accounting for the interparticle electrostatic repulsion could be relevant to avoid misleading interpretations of the results. The use of the ionic initiator in the microgel synthesis, even in small quantities as that used in the KPS0.1 microgel system, provokes the appearance of a residual charge in the PNIPAM polymer chains that is reflected on the measured structure factors.

To carry out the crystallization study, we chose the samples prepared at $n = 5.94$ particles/ μm^3 for the less charged microgel system KPS01 and $n = 2.39$ particles/ μm^3 for the most charged microgels KPS0.6. At these

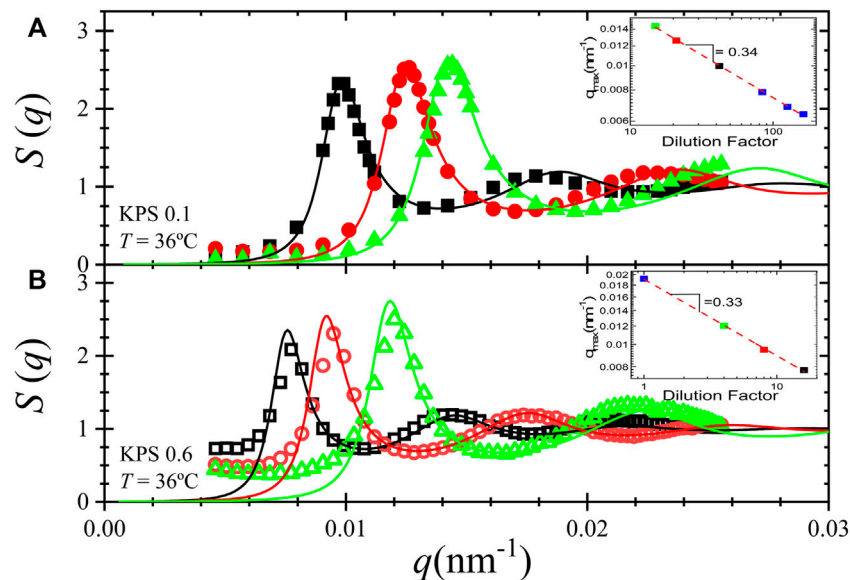


FIGURE 2

Measured static structure factors at 36°C for: (A) KPS0.1 system at $n = 2.94$ particles/ μm^3 (black squares), 5.94 particles/ μm^3 (red circles), and 8.85 particles/ μm^3 (green triangles), (B) KPS0.6 system at $n = 1.34$ particles/ μm^3 (black open squares), 2.39 particles/ μm^3 (red open circles), and 5.06 particles/ μm^3 (green open triangles), along with their HNC calculations (lines). Insets: Main peak position versus dilution factor used to prepare the system from the stock solution. The dashed line is a linear fit in the log-log presentation with a slope of -0.34 for KPS0.1 system and -0.33 for KPS0.6.

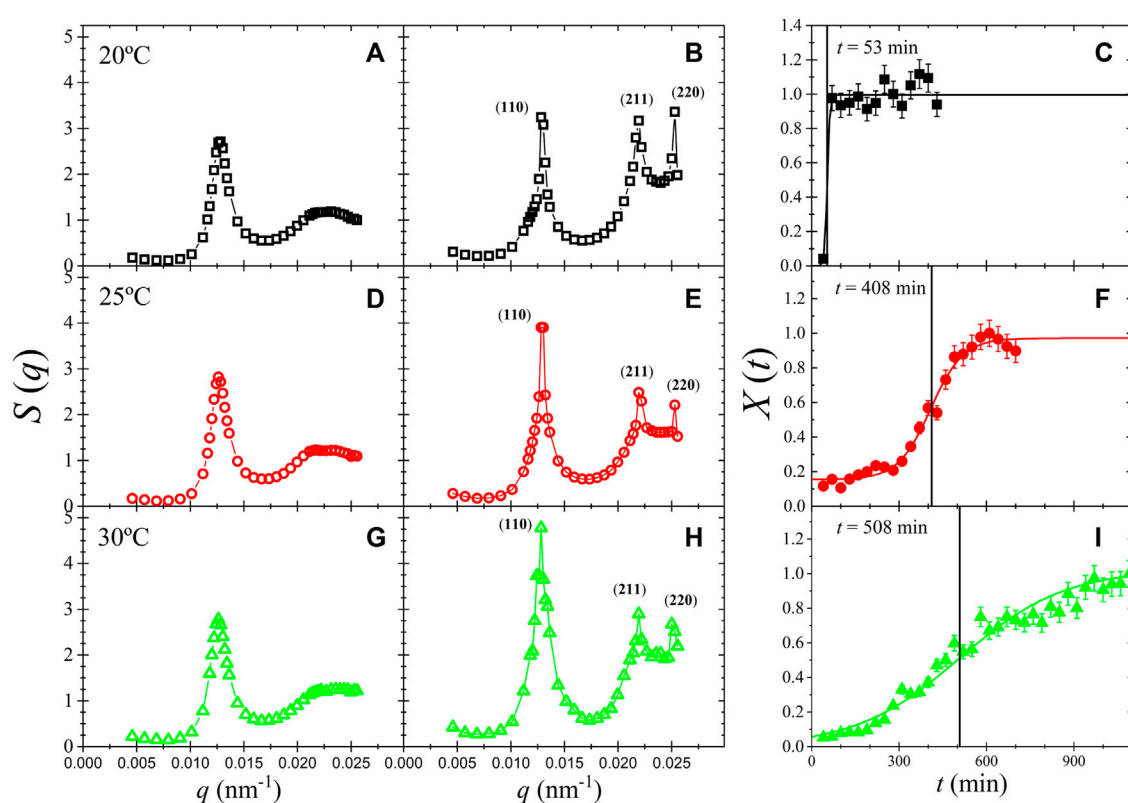


FIGURE 3

(A) Initial measured static structure factor, $S(q)$, right after quenching, (B) Final equilibrium static structure, (C) time evolution of the degree of crystallinity (symbols) along with a Boltzmann fit (continuous line) at 20°C. (D) Initial $S(q)$ right after quenching, (E) Final equilibrium static structure, (F) time evolution of the degree of crystallinity (symbols) along with a Boltzmann fit (continuous line) at 25°C. (G) Initial $S(q)$ right after quenching, (H) Final equilibrium static structure, (I) time evolution of the degree of crystallinity (symbols) along with a Boltzmann fit (continuous line) at 30°C for sample KPS0.1 at $n = 5.94$ particles/ μm^3 .

concentrations, the systems are in the liquid phase at high temperatures, and the crystallization process can be followed in time at lower temperatures. Notice that a more diluted sample was chosen for the more charged system because, at higher concentrations, the samples crystallize so quickly that the crystallization kinetics could not be followed. This fact confirms that the higher the initiator used in the synthesis, the higher the microgel electrostatic charge. Conversely, at lower particle concentrations, either microgel dispersions do not crystallize at low temperatures, or the crystallization is too slow to be followed experimentally. Therefore, after confirming that our sample was in the liquid state at 45°C, we carried out the quenching from 45°C to lower temperatures by placing the sample, previously heated up to 45°C, on the decalin bath of the light scattering device that was at 20°C, 25°C, and 30°C, respectively. Then, the sample was left there for 10 min to assure thermal equilibrium at the desired temperature, and the crystallization of the system was followed by measuring the temporal evolution of the $S(q)$. The initial $S(q)$ measured right after the equilibration time

shows a liquid static structure for all the investigated temperatures, as shown in Figure 3 for the KPS0.1 sample. The initial $S(q)$ measured at 20°C, 25°C, and 30°C are plotted in Figures 3A,D,G; respectively. Notice that, right after quenching, the samples show a liquid-like structure, but the main peak height of the $S(q)$ is above 2.85, thus indicating that the sample will eventually crystallize as predicted by the Hansen-Verlet freezing criterion for monodisperse systems [37]. Indeed, the sample static structure evolves to its final equilibrium state, corresponding to a crystalline phase, as shown in Figures 3B,E,H for 20°C, 25°C, and 30°C; respectively. Moreover, the appearance of iridescence highlights the crystallization of the sample. At all temperatures, the microgel dispersion displays a body-centered cubic crystalline (BCC) structure, identified by the Miller indexes corresponding to the Bragg peaks appearing in the structure factor. Previous simulations [38] and experiments [4], performed for systems at low particle concentrations displaying long-range repulsive interparticle interactions, report spontaneous assembling into BCC lattices. To study

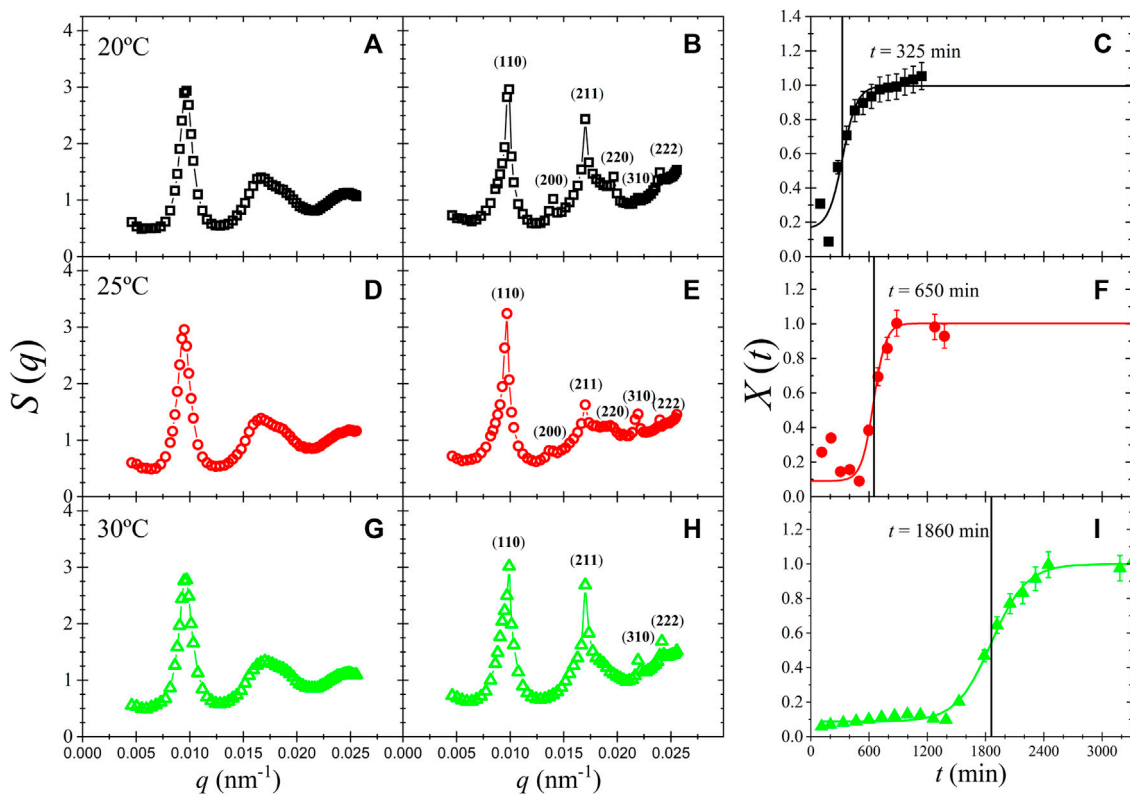


FIGURE 4

(A) Initial measured static structure factor, $S(q)$, right after quenching, (B) Final equilibrium static structure, (C) time evolution of the degree of crystallinity (symbols) along with a Boltzmann fit (continuous line) at 20°C. (D) Initial $S(q)$ right after quenching, (E) Final equilibrium static structure, (F) time evolution of the degree of crystallinity (symbols) along with a Boltzmann fit (continuous line) at 25°C. (G) Initial $S(q)$ right after quenching, (H) Final equilibrium static structure, (I) time evolution of the degree of crystallinity (symbols) along with a Boltzmann fit (continuous line) at 30°C for sample KPS0.6 at $n = 2.4$ particles/ μm^3 .

the crystallization evolution, we determine the time dependence of the sample structure by measuring the $S(q)$ at different times.

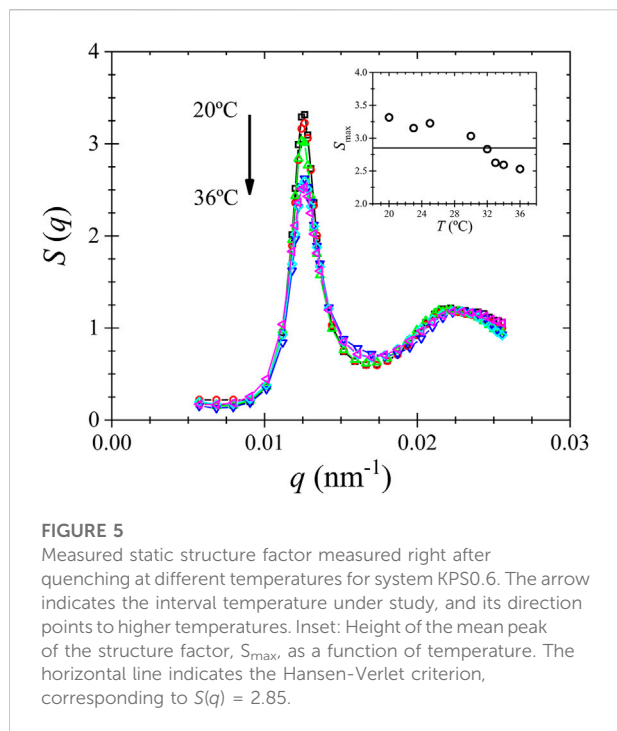
Interestingly, the naked eye can observe differences in the crystallization kinetics since the sample quenched to 20°C crystallizes faster than that at 25°C, and the latter is faster than that at 30°C. As the final equilibrium state is deeper into the crystal region and farther from the liquid-crystal transition, the crystallization kinetics is faster. To quantitatively analyze the crystallization kinetics, we calculate the degree of crystallization, $X(t)$, by using

$$X(t) = c \int_{q_1}^{q_2} S_c(q, t) dq, \quad (3)$$

Where c is a normalization constant. The static structure factor of the crystalline phase $S_c(q, t)$ is calculated by subtracting the contribution of the background fluid from the measured static structure factor $S(q, t)$. We estimate the contribution from the background fluid by scaling the initial measurement with a factor, $S_f(q, t=0) = \alpha(t)S(q, t=0)$, so that the scattered intensity

matches the background of the measurement at time t , $S_c(q, t) = [S(q, t) - \alpha(t)S(q, t=0)]$ [39]. The time evolution of the resulting degree of crystallization calculated for 20°C, 25°C, and 30°C are shown as symbols in Figures 3C,F,I, respectively. At all temperatures, we can observe three regimes: 1) the first one corresponds to the early states where the crystalline precursor appears, 2) then, the crystallinity increases sharply (crystal growth), and 3) the last region is reached steadily (coarsening) after the crystallization of the whole sample, where $X(t)$ remains almost constant. These crystallinity curves resemble others obtained in crystallization studies performed on different colloidal systems [39]. Based on these results, where a sigmoidal pattern is observed, similarly to other phase-transition phenomena, the degree of crystallization can be reasonably described by a Boltzmann-type function of the form [40].

$$X(t) = \frac{A_1 - A_2}{1 + e^{(t-\tau)/p}} + A_2, \quad (4)$$

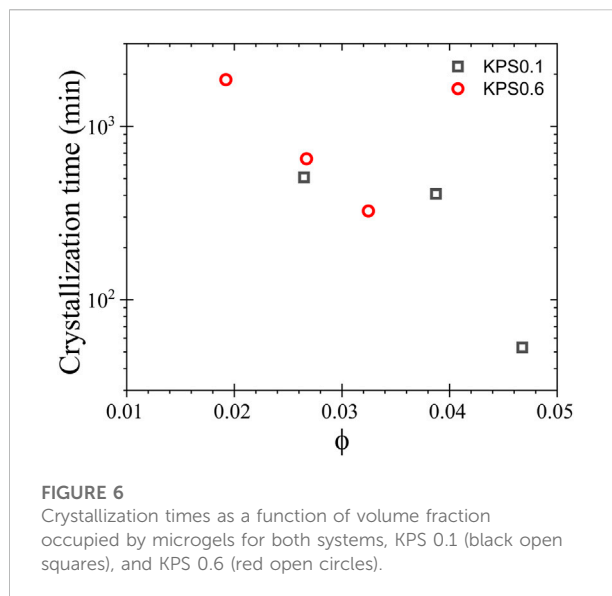


where A_1 , A_2 , and p are constants obtained from the fit, and τ can be identified as a characteristic time for the crystallization of the system, considered as the time where the crystallinity increases faster, as observed in Figures 3C,F,I.

The fits to the $X(t)$, shown as continuous lines in the figure, describe the experiments reasonably well and provide the values of the mean crystallization time τ marked by vertical lines. For the lowest temperature under study, 20°C, the crystallization time obtained is $\tau = 53$ min; then this time increases to $\tau = 412$ min for 25°C and $\tau = 508$ min for 30°C. Note that in the crystallization process, the temperature increase provokes slower.

Kinetics reflected in the increase of the crystallization times and a slowdown of the crystallization rate. Analogously, the same study was carried out for the most charged system, KPS0.6; the results are shown in Figure 4. In this case, the initial $S(q)$ also displays a liquid-like structure with the main peak height higher than 2.85 for all temperatures investigated, as can be seen in Figures 4A,D,G. Similar to the less charged system, the equilibrium state corresponds to a BCC crystal (Figures 4B,E,H).

Additionally, the evolution of the crystallinity factors resembles those obtained for the KPS0.1 system, as shown in Figures 4C,F,I. For the most charged system, the crystallization times are $\tau = 325$ min at 20°C, $\tau = 650$ min at 25°C, and $\tau = 1860$ min at 30°C, represented in the figures by vertical lines. For this system, the crystallization process also slows as the system temperature approximates the temperature where the sample undergoes a liquid-solid transition. The liquid-solid transition temperature of the system is estimated from measurements of the static structure factor at different temperatures, right after



thermal equilibrium. The measured static structure factors are shown in Figure 5. Here, we can observe that the sample structure is more correlated at low temperatures, reflected in the height of the principal peak of $S(q)$, S_{\max} , than at high temperatures.

The decrease in correlation with temperature has been reported previously for deionized charged microgel dispersions [4, 8, 41], and it is associated with an entry of counterions to the microgel as the particle collapses, which translates into a smaller net particle charge [4]. This entry of counterions compensates for the increased electrostatic energy due to the distance reduction between the particles charged groups during microgel shrunk. For those samples showing a $S_{\max} > 2.85$, the measured static structure at initial times corresponds to a metastable state since the sample eventually crystallizes. However, at higher temperatures, around the VPTT and beyond, the initial measured structure corresponds to an equilibrium liquid state. The liquid-solid transition temperature is better observed in the inset of Figure 5, where S_{\max} is plotted as a function of temperature. Notice that the liquid-crystal transition temperature, marked with a horizontal line at 2.85, is around 32°C. The similarity between the values found for the VPTT and the liquid-crystal transition temperature is a coincidence since, for more concentrated systems, an increase of the latter is expected [4].

The crystallization occurs when the initial colloidal fluid is quenched to a temperature beyond the fluid-solid transition boundary. Thus, in both cases, KPS0.1 and KPS0.6 display the expected temperature dependence of the crystallization rate. In Figure 6, the crystallization times are shown for both systems as a function of volume fraction. Here we can observe that, on the one hand, crystallization is faster for the lowest temperature studied, 20°C, because the particle's charge, size and volume fraction become larger than at higher temperatures. At this temperature,

particles fill more space and interact more strongly, thus reducing the free energy of the whole system and favoring crystal formation. On the other hand, at higher temperatures close to but smaller than the liquid-crystal temperature, the free energy of the crystal becomes unfavorably for crystallization. Thus, an increment of environment entropy is required to achieve crystallization, resulting in a slower process. Interestingly, the volume fraction dependence of the crystallization time is very similar for both systems and, apparently, independent of the charge of the microgel. However, in order to confirm this behavior, more experiments are needed.

Concluding remarks

In this work, we study the crystallization kinetics of charged PNIPAM microgels dispersions at deionized conditions. We find that the crystallization rate can be tuned by temperature, resulting from the inherent temperature dependence of PNIPAM that affects microgel size, volume fraction, and particle charge. The crystallization study shows that, independently of the microgel charge, the nucleation time increases as the dimension of the microgel decreases with increasing temperature. The temperature increase provokes changes in the dispersion volume fraction, particle diffusion coefficient, and particle electrostatic charge, being a complex problem worthy of being analyzed. Previously, similar studies have been performed, but in neutral microgel suspensions, where the volume fraction of the dispersions under study was higher than 50% [11]. In our case, the system undergoes a liquid-crystal transition at very low volume fractions, $\sim 1\text{--}5\%$, thanks to the microgels' low polydispersity and electrostatic charge. Another difference between previous studies and ours is how the initial state is reached. In the first, the initial metastable state is achieved by molten shearing once the system is at the desired temperature. However, in our case, the initial liquid phase that assures no memory effects is reached by heating the sample to 45°C and then quenching to the temperature under study. Working with charged microgels under deionized conditions offers the possibility of studying the phenomena of colloidal crystallization at very low volume fractions, which helps to minimize the inherent experimental difficulties associated with

gravity and systems turbidity. We consider that our results encourage further systematic studies as a function of number concentration, temperature, and electrostatic charge in microgels dispersions to describe a complete scenario.

Data availability statement

The original contributions presented in the study are included in the article/supplementary material, further inquiries can be directed to the corresponding authors.

Author contributions

JB-F and DR-C performed the experiments and helped with data analysis. CH-P and LR-O planned the experiments, analyzed data, and wrote the manuscript.

Funding

CH-P and LR-O acknowledge Conacyt (Projects A1-S-16002, A1-S-9197, and INFR-294203) and UAM-Azcapotzalco for financial support.

Conflict of interest

The authors declare that the research was conducted in the absence of any commercial or financial relationships that could be construed as a potential conflict of interest.

Publisher's note

All claims expressed in this article are solely those of the authors and do not necessarily represent those of their affiliated organizations, or those of the publisher, the editors and the reviewers. Any product that may be evaluated in this article, or claim that may be made by its manufacturer, is not guaranteed or endorsed by the publisher.

References

- Hirotsu Y, Hirokawa T, Tanaka T. Volume-phase transitions of ionized N-isopropylacrylamide gels. *J Chem Phys* (1987) 87:1392–5. doi:10.1063/1.453267
- Hu Z. Crystallization of microgel spheres. In: A Fernandez-Nieves, HM Wyss, J Mattsson, DA Weitz, editors. *Microgel suspensions: Fundamentals and applications*. Weinheim, Germany: WILEY-VCH Verlag GmbH & Co (2011). p. 207–28.
- Karg M, Pich A, Hellweg T, Hoare T, Lyon LA, Crassous JJ, et al. Nanogels and microgels: From model colloids to applications, recent developments, and future trends. *Langmuir* (2019) 35:6231–55. doi:10.1021/acs.langmuir.8b04304
- Braibanti M, Haro-Pérez C, Quesada-Pérez M, Rojas-Ochoa LF, Trappe V. Impact of volume transition on the net charge of poly-N-isopropyl acrylamide microgels. *Phys Rev E* (2016) 94:032601. doi:10.1103/physreve.94.032601
- Lyon LA, Meng Z, Singh N, Sorrell CD, John ST. Thermoresponsive microgel-based materials. *Chem Soc Rev* (2009) 38:865–74. doi:10.1039/b715522k
- Alsayed AM, Islam MF, Zhang J, Collings PJ, Yodh AG. Premelting at defects within bulk colloidal crystals. *Science* (2005) 309:1207–10. doi:10.1126/science.1112399

7. Frenzel L, Dartsch M, Balaguer GM, Westermeier F, Grübel G, Lehmkuhle F. Glass-liquid and glass-gel transitions of soft-shell particles. *Phys Rev E* (2021) 104: L012602. doi:10.1103/physrev.104.L012602
8. Aguirre-Manzo LA, Ledesma-Motolinía M, Rojas-Ochoa LF, Trappe V, Callejas-Fernández J, Haro-Pérez C, et al. Accounting for effective interactions among charged microgels. *Phys Rev E* (2019) 100:032602. doi:10.1103/physrev.100.032602
9. Ledesma-Motolinía M, Braibanti M, Rojas-Ochoa LF, Haro-Pérez C. Interplay between internal structure and optical properties of thermosensitive nanogels. *Colloids Surf A: Physicochemical Eng Aspects* (2015) 482:724–7. doi:10.1016/j.colsurfa.2015.07.020
10. Tang S, Hu Z, Zhou B, Cheng Z, Wu J, Marquez M. Melting kinetics of thermally responsive microgel crystals. *Macromolecules* (2007) 40:9544–8. doi:10.1021/ma0716682
11. Tang SJ, Hu ZB, Cheng ZD, Wu JZ. Crystallization kinetics of thermosensitive colloids probed by transmission spectroscopy. *Langmuir* (2004) 20:8858–64. doi:10.1021/la049203h
12. Hellweg T, Dewhurst CD, Brückner E, Kratz K, Eimer W. Colloidal crystals made of poly(N-isopropylacrylamide) microgel particles. *Colloid Polym Sci* (2000) 278:972–8. doi:10.1007/s003960000350
13. Niozu A, Kumagai Y, Hiraki TN, Fukuzawa H, Motomura K, Bucher M, et al. Crystallization kinetics of atomic crystals revealed by a single-shot and single-particle X-ray diffraction experiment. *Proc Natl Acad Sci U S A* (2021) 118: e2111747118. doi:10.1073/pnas.2111747118
14. Zhou J, Cai T, Tang S, Marquez M, Hu Z. Growth of columnar hydrogel colloidal crystals in water-organic solvent mixture. *Langmuir* (2006) 22:863–6. doi:10.1021/la0515773
15. Lapkin D, Mukharamova N, Assalauova D, Dubinina S, Stelhorn J, Westermeier F, et al. *In situ* characterization of crystallization and melting of soft, thermoresponsive microgels by small-angle X-ray scattering. *Soft Matter* (2022) 18:1591–602. doi:10.1039/d1sm01537k
16. Rieese CE, Mikhonin AV, Kamenjicki M, Tikhonov A, Asher SA. Nanogel nanosecond photonic crystal optical switching. *J Am Chem Soc* (2004) 126:1493–6. doi:10.1021/ja037118a
17. Das M, Zhang H, Kumacheva E. Microgels: Old materials with new applications. *Annu Rev Mater Res* (2006) 36:117–42. doi:10.1146/annurev.matsci.36.011205.123513
18. Park JG, Rogers WB, Magkiriadou S, Kodger T, Kim SH, Kim YS, et al. Photonic-crystal hydrogels with a rapidly tunable stop band and high reflectivity across the visible. *Opt Mater Express* (2017) 7:253–63. doi:10.1364/ome.7.000253
19. Go D, Rommel D, Chen L, Shi F, Sprakel J, Kuehne A. Programmable phase transitions in a photonic microgel system: Linking soft interactions to a temporal pH gradient. *Langmuir* (2017) 33:2011–6. doi:10.1021/acs.langmuir.6b04433
20. Zhou J, Wei J, Ngai T, Wang L, Zhu D, Shen J. Correlation between dielectric/electric properties and cross-linking/charge density distributions of thermally sensitive spherical PNIPAM microgels. *Macromolecules* (2012) 45:6158–67. doi:10.1021/ma300454h
21. Mohanty PS, Richtering W. Structural ordering and phase behavior of charged microgels. *J Phys Chem B* (2008) 112:14692–7. doi:10.1021/jp808203d
22. Sennato S, Chauveau E, Casciardi S, Bordini F, Truzzolillo D. The double-faced electrostatic behavior of PNIPAm microgels. *Polymers* (2021) 13:1153–79. doi:10.3390/polym13071153
23. Yang Y, Maldonado-Valderrama J, Martín-Molina A. Temperature and electrostatics effects on charged poly(N-isopropylacrylamide) microgels at the interface. *J Mol Liq* (2020) 303:112678. doi:10.1016/j.molliq.2020.112678
24. Senff H, Richtering W. Temperature sensitive microgel suspensions: Colloidal phase behavior and rheology of soft spheres. *J Chem Phys* (1999) 111:1705–11. doi:10.1063/1.479430
25. Liu J, Schöpe HJ, Palberg T. An improved empirical relation to determine the particle number density of fluid-like ordered charge-stabilized suspensions. *Part Part Syst Charact* (2000) 17:206–12. doi:10.1002/1521-4117(200012)17:5/6<206::aid-ppsc206>3.0.co;2-c
26. Schätzel K. Suppression of multiple scattering by photon cross-correlation techniques. *J Mod Opt* (1991) 38:1849–65. doi:10.1080/09500349114551951
27. Aberle LB, Wiegand S, Staudt W. Suppression of multiple scattered light by photon cross-correlation in a 3D experiment. *Prog Colloid Polym Sci* (1997) 104: 121–5. doi:10.1007/bf01182426
28. Urban C, Schurtenberger P. Characterization of turbid colloidal suspensions using light scattering techniques combined with cross-correlation methods. *J Colloid Interf Sci* (1998) 207:150–8. doi:10.1006/jcis.1998.5769
29. Ojeda-Mendoza GJ, Moncho-Jordá A, González-Mozuelos P, Haro-Pérez C, Rojas-Ochoa LF. Evidence of electrostatic-enhanced depletion attraction in the structural properties and phase behavior of binary charged colloidal suspensions. *Soft Matter* (2018) 14:1355–64. doi:10.1039/c7sm02220d
30. Koppel DE. Analysis of macromolecular polydispersity in intensity correlation spectroscopy: The method of cumulants. *J Chem Phys* (1972) 57: 4814–20. doi:10.1063/1.1678153
31. Johnson CS, Gabriel DA. “Dynamic light scattering” in laser light scattering. New York, United States: Dover Publications (1994). p. 22–35.
32. López-León T, Ortega-Vinuesa JL, Bastos-González D, Elaisari A. Cationic and anionic poly(N-isopropylacrylamide) based submicron gel particles: Electrokinetic properties and colloidal stability. *J Phys Chem B* (2006) 110: 4629–36. doi:10.1021/jp0540508
33. Tauer K, Gau D, Schulze S, Völkel A, Dimova R. Thermal property changes of poly(N-isopropylacrylamide) microgel particles and block copolymers. *Colloid Polym Sci* (2009) 287:299–312. doi:10.1007/s00396-008-1984-x
34. Nägele G. On the dynamics and structure of charge-stabilized suspensions. *Phys Rep* (1996) 272:215–372. doi:10.1016/0370-1573(95)00078-x
35. Haro-Pérez C, Rojas-Ochoa LF, Castañeda-Priego R, Quesada-Pérez M, Quesada-Pérez M, Callejas-Fernández J, et al. Dynamic arrest in charged colloidal systems exhibiting large-scale structural heterogeneities. *Phys Rev Lett* (2009) 102:018301. doi:10.1103/physrevlett.102.018301
36. Verwey EJW, Overbeek JTG. *Theory of the stability of lyophobic colloids*. New York: Elsevier (1948).
37. Hansen JP, Verlet L. Phase transitions of the Lennard-Jones system. *Phys Rev* (1969) 184:151–61. doi:10.1103/physrev.184.151
38. Gu L, Xu S, Sun Z, Wang JT. Brownian dynamics simulation of the crystallization dynamics of charged colloidal particles. *J Colloid Interf Sci* (2010) 350:409–16. doi:10.1016/j.jcis.2010.07.009
39. Iacopini S, Palberg T, Schöpe HJ. Crystallization kinetics of polydisperse hard-sphere-like microgel colloids: Ripening dominated crystal growth above melting. *J Chem Phys* (2009) 130:084502. doi:10.1063/1.3078310
40. Navarro-Verdugo AL, Goycoolea FM, Romero-Meléndez G, Higuera-Ciapara I, Argüelles-Monal W. A modified Boltzmann sigmoidal model for the phase transition of smart gels. *Soft Matter* (2011) 7:5847–53. doi:10.1039/c1sm05252g
41. Moncho-Jordá A, Quesada-Pérez M. Crossover of the effective charge in ionic thermoresponsive hydrogel particles. *Phys Rev E* (2019) 100:050602. doi:10.1103/physrev.100.050602